

# Selective Arterial Spin Labeling (SASL): Perfusion Territory Mapping of Selected Feeding Arteries Tagged Using Two-Dimensional Radiofrequency Pulses

Nigel P. Davies\* and Peter Jezzard

**To date, most perfusion magnetic resonance imaging (MRI) methods using arterial spin labeling (ASL) have employed slab-selective inversion pulses or continuous labeling within a plane in order to obtain maps derived from all major blood vessels entering the brain. However, there is great potential for gaining additional information on the territories perfused by the major vessels if individual feeding arteries could be tagged. This study demonstrates noninvasive arterial perfusion territory maps obtained using two-dimensional (2D) selective inversion pulses. This method is designated “selective ASL” (SASL). The SASL method was used to tag the major arteries below the circle of Willis. A combination of 2D selective tagging and multislice readout allows perfusion territories to be clearly visualized, with likely applications to cerebrovascular disease and stroke. Magn Reson Med 49:1133–1142, 2003. © 2003 Wiley-Liss, Inc.**

**Key words:** perfusion; arterial spin labeling; perfusion territory; 2D RF pulses; brain

The ability to visualize the perfusion territories of major feeding arteries in the brain is potentially important for many clinical applications. In particular, assessments of collateral flow, and the delineation of specific vascular distributions can be very useful in the diagnosis and management of cerebrovascular disease. To date, most perfusion studies carried out by MRI (whether in gadolinium bolus injection studies or arterial spin labeling (ASL) studies) have obtained perfusion maps that include contributions from all the arteries feeding the brain. However, ASL offers the potential to selectively tag individual vessels and thereby map the perfusion territory of each vessel independently.

Previous studies (1,2) demonstrated perfusion imaging using selective labeling by employing a transmit surface coil placed close to either the left or right common carotid artery. However, that method is limited to spatially well-delineated vessels in the neck. In another study using a single coil (3), a slab inversion scheme was used to lateralize labeling in one cerebral hemisphere. That approach was used only to extend angiographic methods, rather than to generate perfusion data, and lacks the desired specificity of individual vessel labeling.

The approach we propose here involves localization of the tagging of spins to individual blood vessels using high-

dimensional, spatially-selective radiofrequency (RF) pulses. We refer to this procedure as “selective ASL” (SASL). Such pulses are able to excite shaped columns of spins (2D pulses) or even shaped volumes (3D pulses), rather than the standard 1D slab. 2D spatially-selective RF pulses (4) have been used previously for a wide range of applications in MRI, including navigator applications (5), and restricted field-of-view (FOV) imaging for EPI applications (6). They have also been employed for angiographic imaging (7), line-scan imaging (8), and cardiac imaging (9–12). In this report we use interactively designed 2D selective RF pulses to tag individual major feeding vessels within the cranium. This approach allows perfusion territories in the brain to be visualized with far greater flexibility and specificity than previous methods. It also may enable the impact of collateral flow to be assessed in cases of obstructive lesions in one or more arteries inferior to the circle of Willis. Although other methods already exist for direct assessment of collateral flow into the circle of Willis, such as MR angiography (MRA) (13–15) and transcranial doppler ultrasonography (TCD) (16), none of these techniques measure the impact of such flow on actual tissue perfusion.

## METHODS

All experiments were performed on a 3.0 Tesla whole-body scanner with a Varian Inova console. A Magnex SGRAD Mk III head gradient insert coil was connected to Siemens GPS gradient amplifiers, producing a maximum gradient strength of 34 mT/m in a minimum rise time of 200  $\mu$ s. A quadrature birdcage RF head coil with an internal diameter of 27 cm was used for all imaging.

### Angiographic Sequence

Each scanning session commenced with the acquisition of a sagittal scout image that was used to plan an MR angiogram. Angiographic images were collected from a region spanning approximately 60 mm below to 20 mm above the circle of Willis, showing the location of the principal feeding arteries of the brain. A time-of-flight flow-compensated spoiled gradient-echo sequence was used with the following parameters: TR/TE/flip = 60 ms/6 ms/60°, matrix = 128  $\times$  128, FOV = 256  $\times$  256 mm<sup>2</sup>, and 15–21 slices of 4-mm thickness. The angiogram data were used to select the location of the target segment of the relevant feeding artery while the subject remained in the magnet. This was achieved, for example, by marking with a cursor two points defining a line coinciding with a segment of the vessel being mapped. The target arteries used for this

FMRIB Center, Department of Clinical Neurology, University of Oxford, John Radcliffe Hospital, Oxford, UK.

Grant sponsor: UK Medical Research Council.

\*Correspondence to: Nigel P. Davies, Ph.D., FMRIB Center, John Radcliffe Hospital, Headington, Oxford OX3 9DU, UK. E-mail: npdavies@fmr.ox.ac.uk  
Received 16 September 2002; revised 12 February 2003; accepted 12 February 2003.

DOI 10.1002/mrm.10475

Published online in Wiley InterScience (www.interscience.wiley.com).

© 2003 Wiley-Liss, Inc.

study were the left and right internal carotid arteries (ICAs).

The vessel identification information was then used to solve the matrix transformation equation relating the default and target positions for placement of the 2D RF pencil pulse. In turn, the transformation matrix was decomposed to reveal the required gradient rotation angles and in-plane translation. This information was then used to generate the necessary gradient, RF amplitude, and RF phase waveforms for the pencil pulse in real time. Note that in this preliminary study, the targeted pencil beam was always chosen to be parallel with the readout slices to minimize any subtraction problems caused by direct excitation of the imaging region by the 2D RF pulse. In the case of the ICA, the carotid siphon offered a convenient choice for tagging. When the subject is positioned supine in the scanner, a straight portion of the carotid siphon is oriented parallel to the axial plane at an angle of approximately  $55^\circ$  to the anterior–posterior direction. It was found to have a mean segment length of approximately 2.5 cm across the subjects scanned. Therefore, a pencil oriented in the axial plane could be targeted parallel with this section of the ICA. In practice it was desirable to orient the pencil in the AP direction of the axial plane, and hence at an oblique angle to the targeted section of the artery.

### 2D RF Pulses

The 2D RF pulses used for this study were based on a constant-angle spiral gradient trajectory with 16 turns and a compensated Gaussian RF amplitude envelope (4,17), with a duration of 16 ms. Details of the theory behind the generation of the pencil pulses are provided in the Appendix. The maximum gradient strength,  $G_{\max}$ , was adjusted in order to produce the desired value of  $d_{FWHM}$  for the pencil profile. In most cases  $G_{\max}$  was chosen to be 17 mT/m, giving a  $d_{FWHM}$  of 10.6 mm (easily encompassing a typical vessel diameter of 3–5 mm) and a side lobe radius of 139 mm, thus placing the side lobes outside of the head. The RF pulse amplitude required to produce a  $180^\circ$  flip angle at the center of the Gaussian profile was calibrated along the length of the RF coil to account for inherent  $B_1$ -field inhomogeneities. The appropriate amplitude was then used for each 2D RF pulse depending on the position of the required tag profile.

### SASL Acquisition

A pulse sequence diagram showing the SASL sequence is shown in Fig. 1. The tag module consists of three identical 2D RF pulses separated by a short time interval, which allows blood inverted by a given tag pulse to flow out of the tagging region before the subsequent tag is played out. This strategy increases the time-width and hence the inversion efficiency of the tag bolus. A pulse repetition time (PTR) of 96 ms is used for the ICA tags, which allows the blood to travel the 2.5-cm length of the tagged section if a mean blood velocity of  $\geq 26$  cm/s in the target segment is assumed.

A control condition is also required in order to subtract the effects that are not related to perfusion. The control condition consisted of playing out the 2D gradient wave-

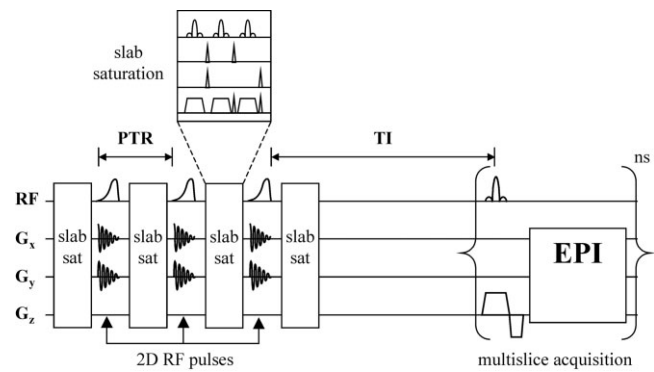


FIG. 1. Timing diagram for SASL sequence. A triple saturation pulse is applied across a slab covering the image slices with alternating crusher gradients to null the signal, immediately followed by the tag module consisting of three spiral 2D RF pulses played out at the desired PTR and interspersed with additional slab saturation modules. This is followed by a multislice EPI readout module after an inflow time (TI). In the control module, the 2D pulse gradients are played out with zero RF amplitude to mimic the eddy current effects of the tag module.

forms with zero tagging RF power. To minimize the effect on the readout slices of direct excitation from the tagging module, a slab incorporating the slices of interest was presaturated immediately before the tag module and between each individual tag pulse in both the tag and control conditions. Following the tag module, an inflow delay time, TI, was inserted to enable tagged spins to move from the tagging region to the tissue slices under examination. Preliminary experiments to investigate the optimum TI when tagging the chosen ICA section in one subject indicated that a value close to  $TI = 2$  s produced the largest perfusion signal. This value was then used for all subsequent subjects. After the in-flow time, an echo-planar imaging (EPI) signal readout module was used to map out the perfusion signal. Flow-crushing gradients were not used, since the vascular signal is expected to be insignificant at this TI. Typical sequence parameters were TR/TE/TI/flip = 2.5 s/20 ms/2 s/ $90^\circ$ , matrix =  $64 \times 64$ , and FOV =  $256 \times 256$  mm<sup>2</sup>. A minimum of 75 tag and control pairs were collected for averaging, which resulted in a scan time of approximately 6 min for mapping a single territory. Five axial slices (6 mm thick, with a 9-mm gap) were acquired sequentially at 80-ms intervals with TI being measured to the first slice. The central slice position was chosen to be approximately at the midpoint of the corpus callosum, as seen on the sagittal scout image. The gap between the most inferior slice and the tag region was typically 30 mm. The power deposition resulting from the saturation and 2D RF pulses was calculated to be approximately 0.1 W/kg, well within safety guidelines.

For the human studies, five normal volunteers (three males and two females,  $30 \pm 5$  years old) were examined. The study was approved by the local ethics committee, and informed consent was provided by all subjects. For each study, perfusion maps were obtained from one or both of the left and right ICAs.

### Reference Perfusion Acquisition

As a comparison, a standard PICORE (Proximal Inversion with Correction for Off-Resonance Effects) perfusion map (18) was also acquired in one subject in order to compare the tagging efficiency of the SASL method with this previously used approach. This was achieved by selecting a PICORE tagging slab thickness that was estimated to tag an amount of blood equivalent to that tagged by the SASL tagging module, and with a similar tag-to-slice block gap. Clearly, however, in the case of the PICORE acquisition, all feeding arteries were tagged. The acquisition parameters used for the PICORE experiment were  $TR/TE/TI = 2.5\text{ s}/20\text{ ms}/2\text{ s}$ , matrix =  $64 \times 64$ , FOV =  $256 \times 256\text{ mm}^2$ , inversion slab thickness = 60 mm, and tag-to-slice block gap = 30 mm.

### Analysis

Perfusion was assessed by taking the mean of the pairwise difference of the control and tag images, and normalizing this to the baseline images taken with no presaturation or tagging. Thus, a percentage change in signal could be measured with a region of interest (ROI) analysis of the normalized mean pairwise difference image, using the Medx (Sensor Systems Inc., Sterling, VA) image analysis package. To assess the signal change within the perfusion territories, each ROI was defined manually on the baseline ( $M_0$ ) image slices to include the expected perfusion territory of the left and right ICAs. This was carried out with reference to the expected territories found in a standard atlas (19). These ROIs were then used to calculate the mean and standard deviation (SD) of the percentage signal change on the normalized mean pairwise difference images for each territory, as well as its contralateral territory. However, given the lack of a sharp definition of the territory borders, and the expected natural variability in the general population, a quantitative spatial comparison of the experimental and reference map was not viable. This also limited the reliable and objective quantification of the signal in the perfusion territories.

### Phantom Experiments

Preliminary phantom experiments were also performed using the SASL sequence to assess the impact of artifacts. For the phantom experiments a 20-cm-diameter gel-filled sphere was used. The use of the 2% agar gel allowed us to assess subtraction errors, including those due to magnetization transfer effects. These experiments were carried out after the perfusion territory was mapped in two subjects, using identical positioning of the 2D RF pulses and read-out slices. In these cases the  $d_{FWHM}$  of the pencil was 10.6 mm and the radius of the first side lobe was 139 mm. All other sequence parameters were kept the same as for the SASL acquisition. The  $T_1$  and  $T_2$  values for the gel phantom were measured to be  $1250 \pm 20\text{ ms}$  and  $115 \pm 10\text{ ms}$ , respectively, providing a close match to the values observed for gray matter at 3 T.

### Flow Simulations

The design algorithms for 2D RF pulses do not account for motion of the spins during ployout of the RF pulse. There-

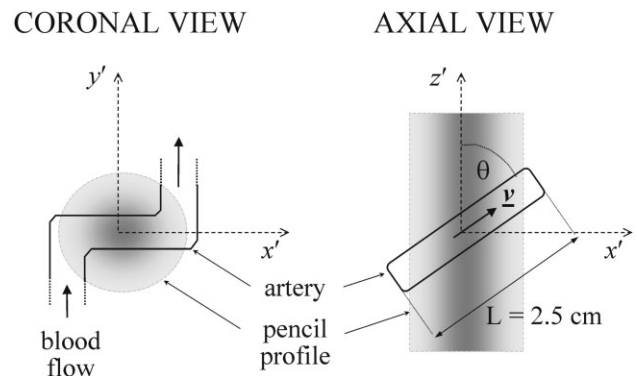


FIG. 2. Illustration of the simple model used to estimate the inversion efficiency of the spiral 2D RF pulse for blood spins in the target section of the ICA flowing at an angle  $\theta$  to the pencil direction.

fore, we conducted simulations to estimate the effect of both constant and pulsatile blood flow in the target artery on the inversion efficiency of the 2D RF pulses. Figure 2 illustrates the geometrical 2D model that was developed as the basis for these simulations. This model is an approximation of the intersection of the 2D pencil with the ICA segment chosen for labeling in this study, as described above. In our initial experiments the spiral gradient waveforms were maintained along the pure gradient axes. This was done to minimize errors in the positioning of the pencil when the gradient coordinate frame is rotated, which can result from differential group delays in gradient waveform propagation to the different axes (although with accurate calibration it is possible to avoid this problem). As a consequence of this, when the carotid siphon was tagged, the 2D tagging profile ( $z'$  axis) was typically oriented at an angle of approximately  $55^\circ$  relative to the direction of blood flow. However, the model allows a variable angle between the pencil and blood flow direction in the tagged segment. This feature was used to investigate the effect on the inversion efficiency of constraining the relative orientation of the tagging profile to the artery.

All simulations were performed with Bloch simulation code written using MATLAB (The MathWorks Inc., Natick, MA). The Bloch equations in the presence of a  $B_1$  field, expressed in the rotating frame, were solved incrementally using the RF amplitude waveform and precalculated values for the off-resonance frequency. The applicable off-resonance value at each time increment was calculated from the known gradient waveforms and the predicted position of the blood relative to the  $x'$  and  $y'$  axes throughout the pulse, based on the blood velocity and model artery geometry. The result of this analysis yields the degree of inversion produced at arbitrary intervals along the blood bolus for a given blood flow velocity. Scheel et al. (20) reported blood flow velocities in the ICA that ranged from about  $26 \pm 5\text{ cm/s}$  at end diastole to  $72 \pm 18\text{ cm/s}$  at peak systole, for healthy adults 20–39 years old. The time-averaged velocity in the vessel center in this group was reported to be  $39 \pm 7\text{ cm/s}$ . Hence, the simulation procedure described above was conducted for blood flow parallel and perpendicular to the pencil direction (i.e., along the  $z'$  and  $x'$  axes, respectively) at velocities of 0 cm/s, 40 cm/s, and 80 cm/s.

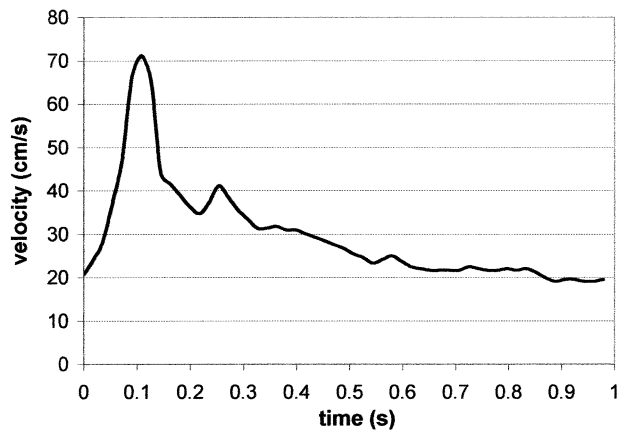


FIG. 3. Example blood velocity waveform in an ICA of one subject over a single cardiac cycle measured using a Doppler ultrasound probe.

Since the blood flow in the arteries of interest is in reality pulsatile, and the cardiac cycle period does not in general match the repetition period of the perfusion pulse sequence, the blood velocity in the artery will in fact be different for successive tag modules. Therefore, the model was extended to estimate the effect of pulsatile flow on the inversion efficiency of repeated 2D RF pulses during a SASL sequence. In order to achieve this, the blood flow velocity in the ICA of a typical subject over one cardiac cycle was measured using an ATL model HDI 5000 SonoCT vascular ultrasound system, corrected for oblique insonation angle. This waveform (shown in Fig. 3) was used as the basis for a simulation of the three-pulse module SASL perfusion experiment described above. The simulation for each individual pulse was carried out in the same way as for the case of constant flow, but with the velocity taken from the appropriate portion of the ICA velocity waveform. For simulation of the first pulse of tag module 1, the mean velocity of the first 16 ms of the velocity waveform was calculated. The distance traveled by the blood during the interpulse interval was then calculated from this and the subsequent 80 ms of the velocity waveform ( $= \int v(t)/dt$ ). For the next pulse in the tag module, the mean velocity of the next 16-ms portion of the velocity waveform was used. This process was repeated for each subsequent interval and pulse period. Making the assumption that the cardiac cycle shown in Fig. 3 simply repeats for the entire duration of the experiment, the cardiac waveform was then effectively played out in a loop until the time of the next tag module (a period of  $2 \times TR$  because of the control image), and the predicted blood velocity for the subsequent 2D RF pulses was estimated as above. This procedure was continued for the total number of tag and control pairs, resulting in a series of tag inversion profiles similar to that expected from a real SASL experiment. Such simulations were made for blood flow parallel and perpendicular to the pencil direction (i.e., along the  $z'$  and  $x'$  axes, respectively) and for oblique flow in the  $(x', z')$  plane. Note that when the off-resonance effect is calculated, only the component of blood velocity perpendicular to the pencil (i.e., along the  $x'$  and  $y'$  axes) need be considered. The results of these simulations

yielded an estimate of the average inversion efficiency achieved in the SASL experiments, taking account of the pulsatile flow effects.

## RESULTS

### Simulations

Figure 4 shows the inversion profiles for a single 2D RF pulse resulting from the model simulations for constant flow velocities of 0, 40, and 80 cm/s. The plot in Fig. 4a corresponds to blood flow parallel to the pencil direction ( $z'$  axis) in the tagged segment, while Fig. 4b shows the results for perpendicular flow. As expected, the shape of the inversion profile along the artery for the case of stationary blood in Fig. 4b (solid line) is determined by the Gaussian profile of the pencil in the  $x'$  direction. The corresponding curve in Fig. 4a differs only in that the

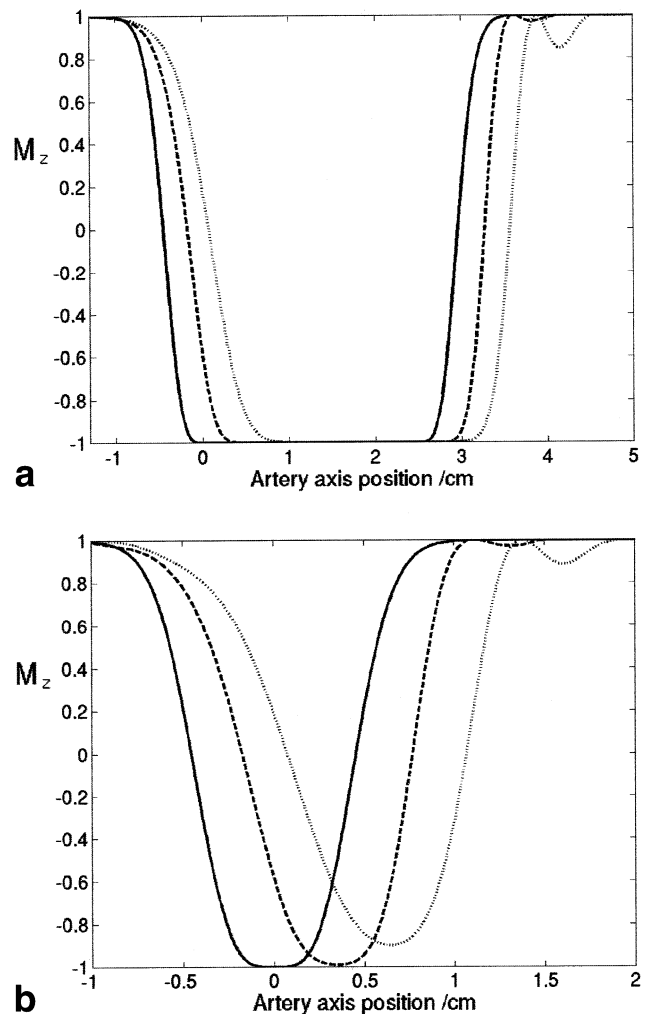


FIG. 4. Simulated inversion profiles using the simple model with (a)  $\theta = 0^\circ$  and (b)  $\theta = 90^\circ$ . Plots show the longitudinal magnetization remaining after the 2D pulse as a function of the position of the spins along the artery axis at the end of the pulse for stationary spins (solid) and spins flowing with velocity 40 cm/s (dashed) and 80 cm/s (dotted). The 2D pulse parameters were:  $G_{\max} = 20$  mT/m,  $T_{\text{pulse}} = 16$  ms, and  $N_{\text{turns}} = 16$ , with an RF envelope as described in the Methods section.

central portion of maximal inversion extends along the length of the segment that is parallel to the pencil direction, and the Gaussian “wings” derive from the pencil profile in the  $y'$  direction. The measured FWHM of the simulated profile is approximately 9 mm. This matches the theoretical value from Eq. [A3], verifying the accuracy of these simulations, where  $G_{\max} = 20$  mT/m,  $N_{\text{turns}} = 16$ ,  $T_{\text{pulse}} = 16$  ms, and  $\beta = 2.3$ . The key comparison in estimating the effect of flow on the inversion efficiency is the total area of the bolus inversion profile. An interesting result, as shown in Fig. 4, is that there is a small increase in the integrated inversion profile for a flow velocity of 80 cm/s relative to the case of 0 cm/s of approximately 3% and 9% for parallel and perpendicular flow, respectively. Simulations over a wider range of velocities (not shown) indicate that the peak increase in integrated inversion profile occurs at approximately 130 cm/s. The integrated inversion profile then decreases to the value obtained for stationary spins at a flow velocity of 200 cm/s. A feature of these simulated profiles is a secondary lobe appearing downstream from the peak that grows as the velocity increases. However, this feature accounts for less than a third of the overall increase in area. For the case of perpendicular flow, the degree of maximum inversion decreases slightly as the velocity increases (5% reduction at 80 cm/s). However, this does not constitute a reduced inversion efficiency for this range of velocities and these pencil parameters.

Figure 5 shows examples of the effect of pulsatile flow on the inversion profiles for tag modules simulated using the model with flow along the  $z'$  axis (Fig. 5a) and flow at  $55^\circ$  to the  $z'$  axis (Fig. 5b). The 2D RF pulse parameters used were the same as in Fig. 4, except that  $G_{\max} = 17$  mT/m for the oblique flow simulation so that it matched the experimental conditions used in this study for tagging the ICA. The plots shown were taken from a simulation consisting of 30 consecutive tag-control pairs. Note that each tag module consists of three 16-ms 2D RF pulses separated by 80 ms. The horizontal axis of these plots represents the relative position along the axis of the artery at the end of the tag module. The upper panel in each case corresponds to tag module 1, applied at the start of the blood velocity cardiac cycle shown in Fig. 3. The second of the 2D RF pulses in this module occurs at a time close to the systolic peak of the blood velocity waveform. Consequently, the inversion profiles resulting from each pulse in the module are most widely distributed along the artery for this tag condition. The lower panel in each case shows tag module 9, where the cardiac cycle in this instance has reached the end-diastolic phase and the blood velocity is at a minimum. In this case, the distance traveled by the blood between the pulses is insufficient to prevent overlap of the individual inversion profiles. This overlap is greater for the case of parallel flow, in which the individual inversion profiles are wider. In this situation, the magnetization history effects of the spins experiencing more than one pulse lead to a reduction in the inversion efficiency. The tag inversion efficiencies for the two modules were calculated to be 101% and 52%, respectively. Over the entire simulation the mean inversion efficiency was calculated to be 72%. For the case of oblique flow, the overlap between the individual tag profiles was mainly in the tails,

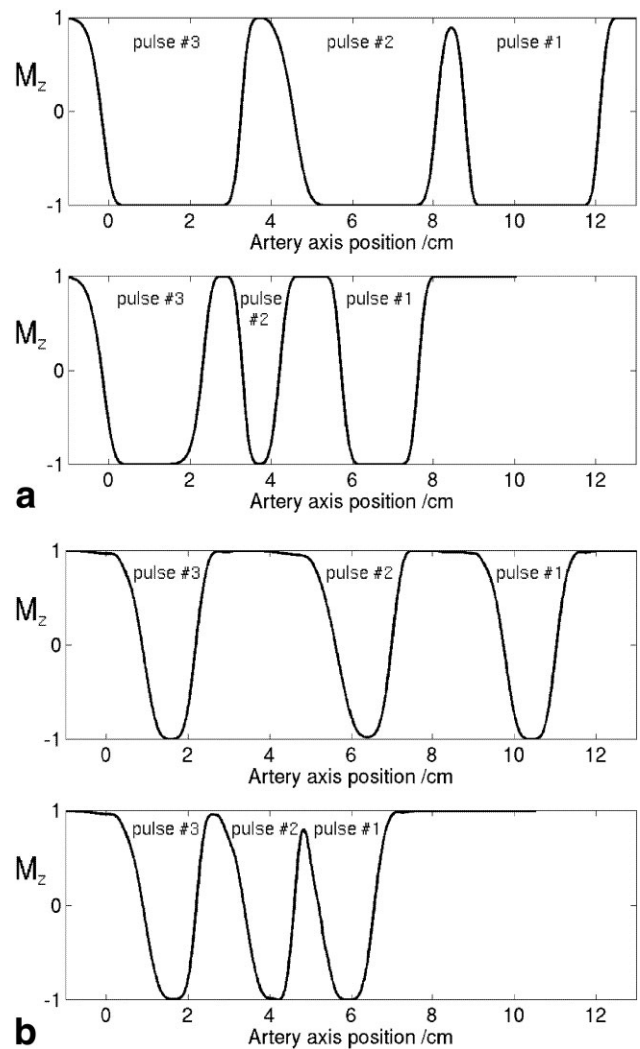


FIG. 5. Simulated inversion profiles vs distance along the model artery for pulsatile flow with (a)  $\theta = 0^\circ$  and (b)  $\theta = 55^\circ$ . Plots represent the inversion profiles of two tag modules taken from a run of 30 in a model perfusion experiment, with each tag module consisting of three 2D RF pulses repeated at 96-ms intervals. In each plot the top panel corresponds to a tag module applied in the systolic phase (high velocity), and the bottom panel corresponds to a tag module applied in the diastolic phase (low velocity) of the cardiac cycle.

and hence the magnetization history of the spins had much less effect on the inversion efficiency. Overall, the simulations revealed a mean inversion efficiency of 100.5% relative to the case of zero blood velocity. However, taking into account the volume of blood tagged, the inversion efficiency of the oblique relative to the parallel flow simulations was 55%.

#### Phantom Experiments

Residual direct excitation effects were estimated by applying the protocol to the gel phantom with the same image slice and 2D labeling pulse positions as were previously applied in the human studies. For the case of a tagging pencil oriented parallel to the readout slices, these valida-

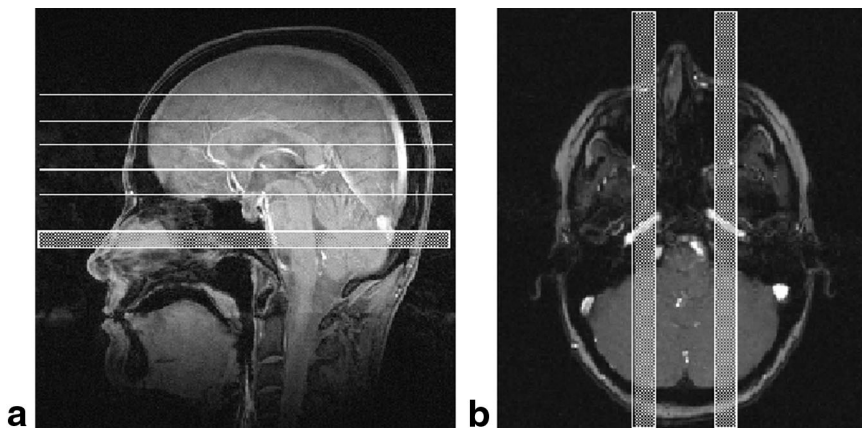


FIG. 6. **a:** Example sagittal scout image with lines indicating the five slice positions for the SASL perfusion images, and the cross-hatched box indicating the 2D tag position for the ICA. **b:** One axial slice from the angiographic sequence at the level of the targeted segment of the ICA, with the cross-hatched boxes indicating the 2D tag positions for the left and right ICAs.

tion experiments revealed residual direct excitation effects of  $<0.02\%$  in slices more than 20 mm above the center of the defined tag region (having a  $d_{FWHM}$  of  $\sim 10$  mm). The position of the excitation due to the first side lobe was outside the phantom.

#### Human Experiments

An indication of the typical locations of the 2D tag region and axial image slices is given in Fig. 6. Figure 6a shows a sagittal localizer image from one of the subjects, with the approximate positions of the prescribed 2D tag region and readout slices marked. In this example the most inferior slice of the multislice readout is approximately 30 mm above the center of the tag region (which has an FWHM of about 10 mm), and therefore the most superior slice is

approximately 90 mm above (still well below the position of the aliasing side lobe at about 140 mm). An axial slice from the angiographic dataset is shown in Fig. 6b, corresponding to the longitudinal position of the tag regions that contain the left and right ICAs. It can be seen that the orientation of the 2D pencil profile, indicated by the shaded region in each image, is at an angle of approximately  $55^\circ$  to the direction of flow in each ICA.

Figure 7 shows the results from a representative individual. The top four slices of the multislice EPI readout are depicted across the top panel, followed by the mean difference images, normalized to the baseline EPI signal ( $\Delta M/M_0$ ). The data shown correspond to 2D tags applied to the right and left ICAs. Despite the low signal-to-noise ratio (SNR), a good discrimination of the expected perfusion

FIG. 7. The four superior slices of baseline EPI readout ( $M_0$ ) from one subject (top panel). Also shown are mean pairwise difference images normalize to baseline EPI ( $\Delta M/M_0$ ) resulting from a 2D tag applied to the right ICA (middle panel) and the left ICA (bottom panel).

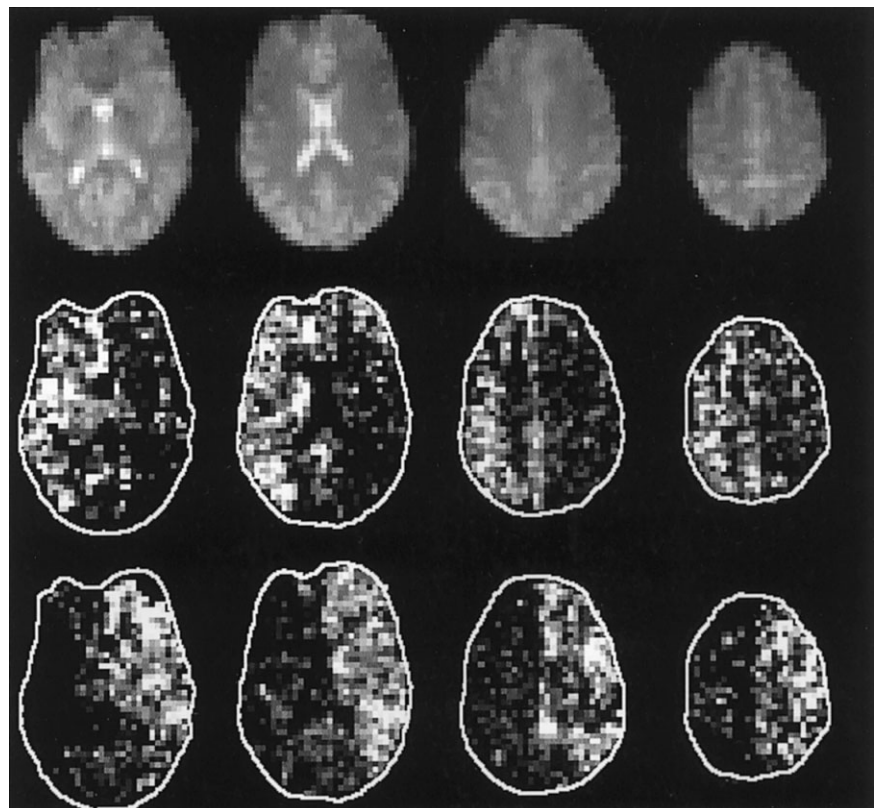
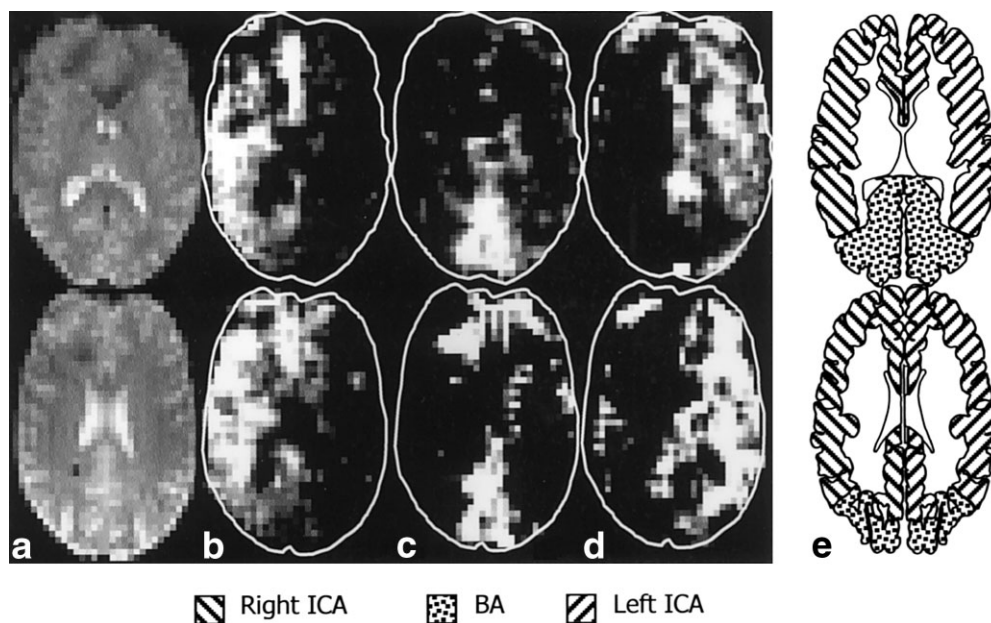


FIG. 8. Slices 2 and 3 from a single individual showing (a) the baseline EPI images ( $M_0$ ), the smoothed normalized mean pairwise difference images ( $\Delta M/M_0$ ) resulting from a 2D tag applied to (b) the right ICA, (c) the basilar artery, and (d) the left ICA. e: The reference perfusion territory maps (adapted from Ref. 19). For the basilar artery, a 2D pulse with an ellipsoidal profile was used ( $10.6 \text{ mm} \times 21 \text{ mm}$ ), oriented in the anterior-posterior direction.



territory is displayed in the relative difference images, with high gray/white matter contrast (particularly evident in the more superior slices). In the more inferior slices, the deep gray matter structures show a high perfusion signal, which may account for the lack of such a clear gray/white matter contrast in these slices.

Figure 8 shows baseline ( $M_0$ ) EPI images (no presaturation or labeling pulses) at two of the slice locations (Fig. 8a), together with the respective perfusion territory maps defined as  $\Delta M/M_0$ , where  $\Delta M$  = the mean pairwise (control-tag) image, obtained by tagging the right (Fig. 8b) and left (Fig. 8d) ICAs in the same subject. Also shown in Fig. 8c is the perfusion territory obtained by tagging the basilar artery, which was attempted in this subject (subject C). Textbook territory maps of the relevant artery systems from closely matched slice locations (Fig. 8e) are shown

for comparison (adapted from Ref. 19). The most inferior slice shown was approximately 30 mm above the center of the tag and 20 mm above the circle of Willis.

Table 1 shows the percentage signal change ( $100\% \times \Delta M/M_0$ ) taken from regions of interest (ROIs) that correspond to cortical areas in the indicated perfusion territories. Results for each subject are shown. Each slice was analyzed separately for each subject, and the mean percentage signal change across all slices was taken for each perfusion territory. The same analysis was carried out for the contralateral regions in each case. As shown in Table 1, the mean signal change for all subjects was approximately  $0.21\% \pm 0.04\%$  for the SASL procedure. The comparison PICORE acquisition used an inversion slab of 60-mm thickness, and the same 30 mm gap between the inversion slab and the image slices. The PICORE protocol yielded a

Table 1  
Mean Perfusion Signal Values From an ROI Analysis of Each Image Slice From the SASL Protocol Applied to Eight Arterial Perfusion Territories in Five Subjects\*

Subject	Tagged artery	SASL signal ( $\Delta M/M_0$ ) %	
		Expected perfusion territory	Contralateral territory
A	Left ICA	$0.20 \pm 0.09$	$0.08 \pm 0.07$
B	Left ICA	$0.19 \pm 0.09$	$0.07 \pm 0.08$
C	Left ICA	$0.22 \pm 0.27$	$0.11 \pm 0.24$
C	Right ICA	$0.14 \pm 0.11$	$0.07 \pm 0.11$
D	Left ICA	$0.21 \pm 0.13$	$0.10 \pm 0.12$
D	Right ICA	$0.22 \pm 0.08$	$0.14 \pm 0.08$
E	Left ICA	$0.22 \pm 0.20$	$0.12 \pm 0.15$
F	Left ICA	$0.28 \pm 0.20$	$0.13 \pm 0.19$
Mean $\pm$ mean (SD)		$0.21 \pm 0.15$	$0.10 \pm 0.13$
SD of means		0.04	0.03
Gel phantom		<0.02	NA
PICORE signal ( $\Delta M/M_0$ ) %			
Left ICA		Right ICA	Mean
$0.30 \pm 0.06$		$0.33 \pm 0.07$	$0.32 \pm 0.07$

\*One subject scanned twice, A and D. The mean signal change within the ROI is quoted for each subject, along with the SD within the ROI.

mean perfusion signal change ( $100\% \times \Delta M/M_0$ ) of  $0.32\% \pm 0.07\%$ . The measurement of the contralateral gray matter regions that are not expected to be perfused by the selected arteries yielded a mean percentage signal change of approximately  $0.10\% \pm 0.03\%$ .

## DISCUSSION

There was good qualitative agreement between the textbook theoretical perfusion territory maps and the experimental results obtained using the SASL method. However, given the method's inherent variability, as described above, it remains to be validated in future studies using intraarterial injection of radioactive microspheres in an animal preparation, or in humans undergoing intracarotid amobarbital testing by selective injection of a radiotracer and subsequent single photon emission-computed tomography (SPECT) or positron emission tomography (PET) scanning (21).

Some contralateral signal change was observed in areas that were not expected to be perfused by the target vessel (based on the atlas territory maps). Table 1 shows that the level of this signal change in vivo was significantly higher than the estimated direct excitation effect from the phantom results. There are three possible explanations for this. First, the contralateral signal could be caused by inadvertent labeling of nonselected arteries. This unintended labeling could come about as a result of flow-induced "aliasing" of the 2D RF pulse, or as a result of distortion of the intended inversion profile caused by an inhomogeneous  $B_0$  field. The precise inversion profile achieved in vivo is difficult to assess directly due to the anatomy of the tagging region. Simulations based on  $B_0$ -field maps from three subjects (not shown) reveal that distortion of the 2D RF pulse profile due to off-resonance effects may account for at least part of the contralateral signal. Conversely, other simulations involving a range of physiological flow conditions at locations remote from the intended selective volume have failed to show any significant aliasing effects. Second, the contralateral signal may be evidence of a contribution to the perfusion of these regions from collateral flow in the communicating arteries of the circle of Willis. In healthy subjects there is expected to be little or no collateral flow. However, the variable configuration of the circle of Willis in the population could lead to apparent collateral flow signal in some subjects. For example, in 10% of the population, both anterior cerebral arteries are supplied by a single ICA (14). The SASL technique may therefore offer an insight into the role played by the circle of Willis in both healthy individuals and those with cerebrovascular disease. These findings could be validated by comparison with X-ray angiography using intraarterial dye injections. Finally, the increased contralateral signal in the in vivo data relative to the phantom data could be the result of physiological noise leading to poor control cancellation.

Table 1 shows that a similar SASL response was observed in the relevant perfusion territory in most of the studies; however, it can be seen that the results from subject C imply a large hemispheric variation. This latter observation is likely due to differences in the efficiency of the 2D inversion pulses in this preliminary technical dem-

onstration, or to differences in the many physiological parameters affecting the perfusion signal. Within each territory, though, the average of the SD is relatively large, at 70% of the mean. This is probably the result of varying partial volume fractions of gray and white matter within each voxel of the ROIs.

On average across the subjects, the perfusion signal measured with the SASL acquisition is approximately 35% lower in the expected perfusion territory compared to the PICORE experiment. However, the comparison is not necessarily informative, since the choice of inversion slab width in the PICORE experiment does not dictate the length of the tag bolus in the ICA in the same way it does in the SASL experiment. In fact, the tag bolus would be expected to be significantly longer than the inversion slab width in the PICORE experiment due to the tortuosity and orientation of the arteries to the tag plane. However, the difference is likely due in part to the inefficient inversion of blood spins that was achieved in the SASL experiments.

The simulations indicate that blood flow does not inherently reduce the inversion efficiency of the 2D pulses. Using the oblique pencil orientation, full inversion was not achieved along the whole length of the targeted artery segment due to the Gaussian nature of the pencil profile, as shown in Fig. 5b. For the pencil width used, the simulated inversion efficiency is accordingly reduced to 55% relative to the parallel case. However, in these preliminary experiments this arrangement offered a more robust solution, for two reasons: First, it allowed the gradient waveforms to be applied along the physical gradient axes, thus removing inaccuracies involved in the rotation step. Second, the geometry and location of other arteries, in particular the contralateral ICA, meant that a pencil oriented parallel with this arterial section would result in some leakage of the tag into neighboring arteries, and therefore in a reduced arterial selectivity (although the use of a 3D pulse could ameliorate this problem). Simulations also showed that inaccurate targeting of the pencil to the artery is more critical in the case of a parallel orientation, since a small error in positioning results in reduced inversion along the entire length of the arterial section. This is because any placement of the tag region slightly off-center with respect to the artery will result in a lower flip angle being applied to the blood spins along the whole length of the tag.

The accuracy achieved in the positioning of the pencil can be inferred from phantom experiments. These have shown that careful accounting for hardware delays in the application of the gradient waveforms is required to allow accurate rotation of the pencil profile. The integrity and accuracy of the offset of the pencil within the plane is dependent on the accuracy and stability of the RF phase produced by the system. This placed a limit on the magnitude of the offset away from isocenter that reliably could be achieved of approximately 50 mm, and the positioning error within this limit was  $< 2$  mm.

In the current implementation, the PTR is fixed and the tag modules occur at different points of the cardiac cycle. When the velocity is too low for fresh blood replacement within the target segment between tag pulses, there is a reduction in the total volume of inverted spins (Fig. 5a, bottom panel). The resulting decrease in the integrated input function to the tissue would reduce the perfusion

signal. At points of high velocity, the chosen TR will be too long, causing the blocks of inverted spins produced by each tag pulse to be spread out in position along the artery (Fig. 5b, top panel). Therefore, some improvements in SASL sensitivity may be gained by employing cardiac gating of the sequence, such that the tagging pulses could be synchronized with a chosen point in the blood velocity cycle within the target artery. If the velocity at this point were known (for example by measurement using phase contrast MRA), the PTR could be set to allow the maximum total inversion volume to be obtained while keeping the time-width of the tag bolus to a minimum. This would also allow the TI to be optimized for the anatomic location of the tag, minimizing the blurring effect caused by the velocity varying between tag modules. The kinetic model for the perfusion signal behavior in SASL will differ from conventional perfusion ASL (PASL) (22) in the nature of the input function. Clearly, in the SASL technique the input function consists of multiple peaks rather than a single rectangle. If the multiple peaks of the input function are spread out, it will lead to a “saw-tooth” effect in the rising edge of the perfusion signal time curve and a reduced peak due to increased relaxation effects. For quantitation purposes, the actual input function could be estimated if the blood velocity were known.

## CONCLUSIONS

In conclusion, we report the acquisition of MR arterial perfusion territory maps in the brain, using 2D RF inversion pulses, to tag individual feeding arteries below the circle of Willis. Territory maps for the left and right ICAs were obtained in five healthy volunteers, and good agreement was observed between the current findings and a standard reference atlas. The method could be a useful adjunct in studies of patients with vascular disease, for which estimates of collateral circulation are desired. It may also be possible to apply the method to examine vessels above the circle of Willis, and to obtain quantitative perfusion territory maps.

## ACKNOWLEDGMENTS

The authors thank Thies H. Jochimsen and Michael von Mengershausen for generously providing software that helped in the design of the 2D RF pulses.

## APPENDIX

### RF Pulse Design

The key concept behind the SASL method is the use of high-dimension RF pulses to spatially constrain the region of selective labeling of the blood magnetization. The design of the 2D spatially selective inversion pulses used in this study was based on the  $k$ -space analysis described by Pauly et al. (4). Although that analysis is strictly valid only for small-flip-angle excitation, it has been shown that for certain RF  $k$ -space trajectories, the perturbation solutions of the Bloch equations for incremental parts of the pulse combine linearly (23). One such  $k$ -space trajectory that allows a linear combination of incremental solutions is the

spiral trajectory. This means that the pulse design method is valid for spiral trajectory pulses of any flip angle. An additional advantage of a spiral trajectory is that it is a natural frame for designing Gaussian-weighted “pencil” profiles with cylindrical symmetry, which are most appropriate in selecting individual arteries, given their geometry.

In our implementation, the prescription of the diameter, position, and orientation of the required pencil profile is made directly from an angiogram showing the major arterial structure. Once a target vector has been defined from the angiographic image (for example, by selecting two points on the desired arterial segment), the required gradient and RF waveforms can be generated in real time to produce an RF pencil pulse that passes through the target locations. The  $B_1$  field modulation required to excite a 2D column of spins is given by (4):

$$B_1(t) = D(k)|\gamma G(t)| \quad [A1]$$

where  $D(k)$  is the Fourier transform of the desired pencil profile to be excited, and  $G(t)$  is the gradient trajectory used to adequately sample RF  $k$ -space. In the present study we use a Gaussian function for  $D(k)$  given by

$$D(k) = \alpha e^{-\beta^2(k_x^2 + k_y^2)/k_{\max}^2}, \quad [A2]$$

A value of  $\beta = 2.3$  was used for all studies, and the gradient strength was adjusted (and hence  $k_{\max}$ ) in order to adjust the radial extent of the pencil inversion pulse. For a spiral  $k$ -space trajectory, the full width at half height of the  $M_z$  pencil profile for a  $180^\circ$  pulse is given by:

$$d_{FWHM} = \frac{4\sqrt{\ln 2}\beta N_{\text{turns}}}{\gamma G_{\max} T_{\text{pulse}}}. \quad [A3]$$

where  $N_{\text{turns}}$  is the number of turns in the spiral trajectory,  $G_{\max}$  is the maximum gradient strength used in the trajectory,  $\gamma$  is the gyromagnetic ratio in Hz/T, and  $T_{\text{pulse}}$  is the duration of the 2D pulse. The position of the first side lobe will occur at a radius given by:

$$r_{sl} = \frac{2\pi N_{\text{turns}}^2}{\gamma G_{\max} T_{\text{pulse}}} \quad [A4]$$

For example, a 16-turn spiral with a duration of 16 ms and a  $G_{\max}$  of 20 mT/m produces a pencil of approximately 9 mm diameter, with aliasing side lobes occurring at a radius of 118 mm. To ensure the minimum amount of contamination of the perfusion signal, therefore, the position of the aliasing side lobes should be outside of the imaging ROI. This places some limits on the position of the 2D tag region with respect to the image slices. The expressions also illustrate a trade-off between choosing a narrower pencil to obtain better vascular specificity and keeping the aliasing side lobes at a sufficient distance to prevent encroachment into the imaging region. If the effect of the aliasing side lobes on the static tissue signal could be effectively nulled or subtracted out with a suitable control pulse, it may be possible to relax this limitation.

A two-step process is used to transform the default position of the pencil profile (aligned along the magnet  $z$ -axis) to lie along the artery. First, the pencil must be rotated such that it is parallel with the target vector. This is achieved by using an appropriate euler angle transformation to rotate the gradient waveform current drives from the magnet frame  $(x, y, z)$  to the frame of the target vector  $(x', y', z')$ , where  $z'$  is aligned along the direction of the target artery. Once the pencil position is aligned to be parallel with the target artery, it can then be shifted within the  $(x', y')$  plane by introducing a phase modulation to the RF waveform that is proportional to the amplitude of the gradient waveforms. It can be shown that the required phase modulation (in radians) is given by:

$$\phi(t) = \frac{r \cdot \gamma G(t) \cdot T_{\text{pulse}}}{N_{\text{turns}}} \quad [\text{A5}]$$

Where  $r$  is the required radial shift and  $G(t)$  is the gradient waveform in the  $(x', y')$  plane. The pencil can then be rotated azimuthally about the  $z'$  axis by incorporating an additional phase offset into the RF phase waveform, determined by the desired rotation angle in the  $(x', y')$  plane. These relationships were confirmed using measurements from pencil pulses applied to a phantom.

## REFERENCES

- Zaharchuk G, Ledden PJ, Kwong KK, Reese TG, Rosen BR, Wald LL. Multislice perfusion and perfusion territory imaging in humans with separate label and image coils. *Magn Reson Med* 1999;41:1093–1098.
- Trampel R, Mildner T, Goerke U, Schaefer A, Driesel W, Norris DG. Continuous arterial spin labeling using a local magnetic field gradient coil. *Magn Reson Med* 2002;48:543–546.
- Eastwood JD, Holder CA, Hudgins PA, Song AW. Magnetic resonance imaging with lateralized arterial spin labelling. *Magn Reson Imaging* 2002;20:583–586.
- Pauly J, Nishimura D, Macovski A. A  $k$ -space analysis of small tip angle excitation. *J Magn Reson* 1989;81:43–56.
- Nehrke K, Bornert P, Groen J, Smink J, Böck JC. On the performance and accuracy of 2D navigator pulses. *Magn Reson Imaging* 1999;17:1173–1189.
- Rieseberg S, Frahm J, Finsterbusch F. Two-dimensional spatially-selective RF excitation pulses in echo-planar imaging. *Magn Reson Med* 2002;47:1186–1193.
- Alley MT, Pauly JM, Sommer FG, Pelc NJ. Angiographic imaging with 2D RF pulses. *Magn Reson Med* 1997;37:260–267.
- Finsterbusch J, Frahm J. Gradient-echo line scan imaging using 2D-selective RF excitation. *J Magn Reson* 2000;147:17–25.
- Hardy CJ, Pearlman JD, Moore JR, Roemer PB, Cline HE. Rapid NMR cardiography with a half-echo M-mode method. *J Comput Assist Tomogr* 1991;15:868–874.
- Cline HE, Hardy CJ, Pearlman JD. Fast MR cardiac profiling with 2-dimensional selective pulses. *Magn Reson Med* 1991;17:390–401.
- Hardy CJ, Bolster Jr BD, McVeigh ER, Iben IE, Zerhouni EA. Pencil excitation with interleaved Fourier velocity encoding: NMR measurement of aortic distensibility. *Magn Reson Med* 1996;35:814–819.
- Pat GTL, Pauly JM, Hu BS, Nishimura DG. One-shot spatially resolved velocity imaging. *Magn Reson Med* 1998;40:603–613.
- Fürst G, Steinmetz H, Fischer H, Skutta B, Sitzer M, Aulich A, Kahn T, Mödder U. Selective MR angiography and intracranial collateral blood flow. *J Comput Assist Tomogr* 1993;17:178–183.
- Hartkamp MJ, van der Grond J, van Everdingen KJ, Hillen B, Mali WPTM. Circle of Willis collateral flow investigated by magnetic resonance angiography. *Stroke* 1999;12:2671–2678.
- Hendrikse J, Hartkamp MJ, Hillen B, Mali WPTM, van der Grond J. Collateral ability of the circle of Willis in patients with unilateral internal carotid artery occlusion: border zone infarcts and clinical symptoms. *Stroke* 2001;32:2768–2773.
- Chaudhuri R, Padayachee RR, Lewis RR, Gosling RG, Cox TCS. Non-invasive assessment of the circle of Willis using transcranial pulsed doppler ultrasound with angiographic correlation. *Clin Radiol* 1992;46:193–197.
- Hardy CJ, Cline HE, Bottomley PA. Correcting for nonuniform  $k$ -space sampling in 2-dimensional NMR selective excitation. *J Magn Reson* 1990;87:639–645.
- Wong EC, Buxton RB, Frank LR. Implementation of quantitative perfusion imaging techniques for functional brain mapping using pulsed arterial spin labeling. *NMR Biomed* 1997;10:237–249.
- Duvernoy HM, Bourgouin P, Cabanis EA, Cattin F. The human brain: surface, blood supply and three-dimensional anatomy, 2nd ed. Vienna: Springer-Verlag; 1998.
- Scheel P, Ruge C, Schöning M. Flow velocity and flow volume measurements in the extracranial carotid and vertebral arteries in healthy adults: reference data and the effects of age. *Ultrasound Med Biol* 2000;26:1261–1266.
- von Oertzen J, Klemm E, Urbach H, Kurthen M, de Greiff A, Linke DB, Biersack HJ, Elger CE. SATSCOM—selective amobarbital test intraarterial SPECT coregistered to MRI: description of a method assessing selective perfusion. *Neuroimage* 2000;12:617–622.
- Buxton RB, Frank LR, Wong EC, Siewert B, Warach S, Edelman RR. A general kinetic model for quantitative perfusion imaging with arterial spin labelling. *Magn Reson Med* 1998;40:383–396.
- Pauly J, Nishimura D, Macovski A. Analytic design of large-tip-angle multidimensional pulses. In: Proceedings of the 8th Annual Meeting of SMR, Amsterdam, The Netherlands, 1989. p 862.